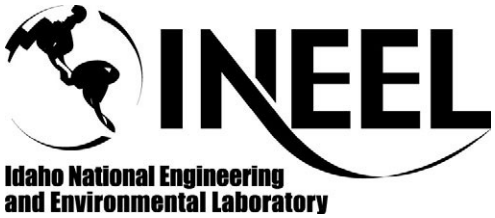

INEEL/CON-04-02510
PREPRINT

Hydrogen Production Using The Modular Helium Reactor

Edwin A. Harvego
SM Mohsin Reza
Matt Richrds
Arkal Shenoy

May 16-20, 2005

13th International Conference On Nuclear Engineering

13th International Conference on Nuclear Engineering
Beijing, China, May 16-20, 2005
ICONE13-50281

HYDROGEN PRODUCTION USING THE MODULAR HELIUM REACTOR

Edwin A. Harvego
Idaho National Laboratory
P. O. Box 1625, Idaho Falls, Idaho 83415
Phone: (208) 526-9544, Fax: (208) 526-2930
e-mail: Edwin.Harvego@inl.gov

SM Mohsin Reza
Texas A&M University
Dept. of Nuclear Engineering
129 Zachry Engineering Center 3133 TAMU
College Station, TX 77843-3133
Phone: (979) 845 4987, e-mail: mreza@cedar.tamu.edu

Matt Richards
General Atomics
P.O. Box 85608, San Diego, CA 92186-5608
Phone: (858) 455-2457, Fax: (858) 455-2596
e-mail: matt.richards@gat.com

Arkal Shenoy
General Atomics
P.O. Box 85608, San Diego, CA 92186-5608
Phone: (858) 455-2552, Fax: (858) 455-2469
e-mail: arkal.shenoy@gat.com

ABSTRACT

The high-temperature characteristics of the Modular Helium Reactor (MHR) make it a strong candidate for the production of hydrogen using either thermochemical or high-temperature electrolysis (HTE) processes. Using heat from the MHR to drive a Sulfur-Iodine (SI) thermochemical hydrogen process has been the subject of a DOE sponsored Nuclear Engineering Research Initiative (NERI) project lead by General Atomics, with participation from the Idaho National Laboratory (INL) and Texas A&M University. While the focus of much of the initial work was on the SI thermochemical production of hydrogen, recent activities have also included development of a preconceptual design for an integral HTE hydrogen production plant driven by the process heat and electricity produced by a 600 MWt MHR.

This paper describes ATHENA analyses performed to evaluate alternative primary system cooling configurations for the MHR to minimize peak reactor vessel and core temperatures while achieving core helium outlet temperatures in the range of 900 ^{o}C to 1000 ^{o}C, needed for the efficient production of hydrogen using either the SI or HTE process. The cooling schemes investigated are intended to ensure peak fuel temperatures do not exceed specified limits under normal or transient upset conditions, and that reactor vessel temperatures do not exceed ASME code limits for steady-state or transient conditions using standard LWR vessel materials. Preconceptual designs for both an SI and HTE hydrogen production plant driven by one or more 600 MWt MHRs at helium outlet temperatures in the range of 900 ^{o}C to 1000 ^{o}C are described and compared. An initial SAPHIRE model to evaluate the reliability, maintainablility, and availability of the SI hydrogen production plant is also described. Finally, a preliminary flowsheet for a conceptual design of an HTE hydrogen production plant coupled to a 600 MWt modular helium reactor is presented and discussed.

1. INTRODUCTION

Because of its ability to produce high-temperature helium, the MHR is well suited for a number of process-heat applications, including hydrogen production. Two hydrogen-production technologies have emerged as leading candidates for coupling to the MHR: thermochemical water splitting using the sulfur-iodine (SI) process and high-temperature electrolysis (HTE). In this paper, we discuss conceptual designs being developed for coupling the MHR to the SI and HTE processes. These concepts are referred to as the SI-based H2-MHR and the HTE-based H2-MHR, respectively [1, 2].

2. PLANT DESCRIPTIONS

The H2-MHR plants being considered consist of one or more 600-MW(t) reactor modules, with each module coupled to a hydrogen production plant. For the SI-based H2-MHR, all 600 MW of thermal energy is transferred through an intermediate heat exchanger (IHX) to a secondary helium loop

that interfaces with the SI hydrogen production plant. For the HTE-based H2-MHR, approximately 90% of the thermal energy is used to produce electricity using a direct Brayton cycle and the remaining thermal energy is used to produce high-temperature steam. Both the electricity and steam are supplied to solid oxide electrolyzers (SOEs) to produce hydrogen. Both concepts have the potential to produce hydrogen economically with efficiencies on the order of 50%.

MHR Reactor System

Figure 1 shows the MHR reactor system. The possibility of a core meltdown is precluded through the use of refractory, coated-particle fuel and nuclear-grade graphite fuel elements with high heat capacity and thermal conductivity, combined with operation at a relatively low power density with an annular core arrangement. For hydrogen production, the core-outlet temperature of the MHR will be increased from 850°C to 950°C. Previous studies indicate it should be possible to increase the coolant-outlet temperature without a proportional increase in fuel temperatures through modest modifications of the reactor internals design to reduce the fraction of bypass flow and optimization of the core physics design to reduce power peaking factors [3].

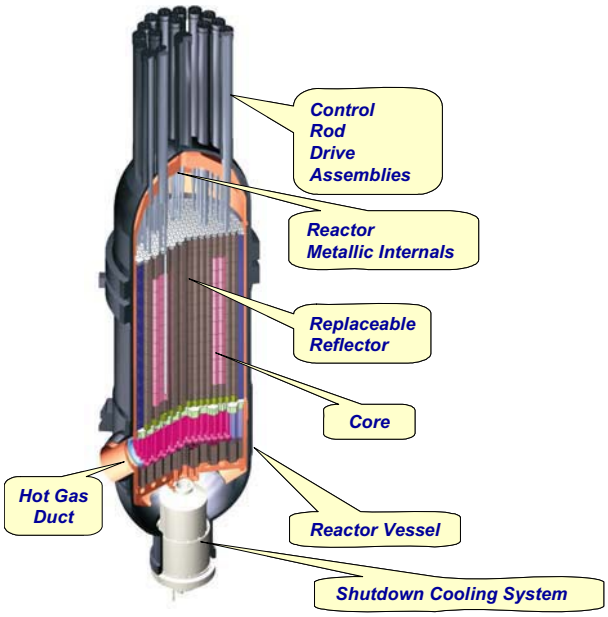

Figure. 1. MHR Reactor System

Sulfur-Iodine Process

As indicated in Figure 2, the SI process consists of three primary chemical reactions that involve decomposition of sulfuric acid and hydrogen iodide, and regeneration of these reagents using the Bunsen reaction. The actual flowsheet for the process is fairly complex and involves significant recuperation of heat to improve efficiency. The plant design based on this process would consist of several modular trains in order to improve reliability. In addition to demonstrating the complex SI-process flowsheet at pilot scale, design of a full-scale IHX operating at temperatures in excess of 900°C may prove to be one of the more challenging issues for interfacing the MHR with the SI process.

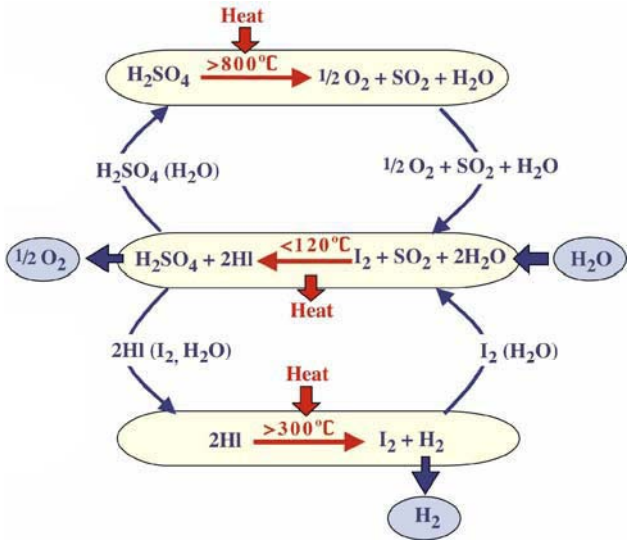

Figure 2. SI Cycle

High-Temperature Electrolysis

The conceptual design of the HTE-based plant would more closely resemble that of a conventional electricity-producing MHR, since about 90% of heat is used to produce electricity. Electricity would be produced using a direct Brayton cycle, but the heat supplied to produce high-temperature steam would be transferred through a secondary helium loop in order to preclude tritium migration into the product hydrogen gas. The current flowsheet, described later, includes recuperation of heat from the hot hydrogen and oxygen product gases to heat the feed water supplied to the steam generator. A potential issue is design of a recuperator that can operate reliably with hot oxygen as one of the process fluids. The SOEs would consist of many modular units. Economics of the process could depend in large measure on cost reductions associated with mass production of the SOE cells.

3. ATHENA CODE CALCULATIONS

The ATHENA code has been developed at the INL to perform thermal-hydraulic system analyses using a variety of fluid properties that might be used in advanced reactors [4]. The ATHENA code is incorporated as a compile time option in the RELAP5-3D computer code [5], which in turn is an extension of RELAP5/MOD3 computer code [6]. The principal difference between RELAP5 and ATHENA is that RELAP5 was designed to use water as the working fluid while ATHENA allows the use of many different working fluids, including helium gas. More detailed information on the ATHENA and RELAP5 codes is contained in References 4 and 5.

Plant Models

ATHENA models have been developed to model the reactor vessel, primary cooling system, and reactor cavity cooling system (RCCS) of the MHR, and the intermediate loop of the SI-based H2-MHR. As part of initial design studies, a number of ATHENA code calculations were performed to evaluate reactor system thermal-hydraulic response under both steady state and transient operating conditions. In particular, sensitivity calculations were performed to determine the effect of changes in reactor coolant flow configurations on peak core and vessel wall temperatures during both steady state and transient operation. Selected results from some of these studies are presented in this section.

Initial calculations using the ATHENA code investigated the potential for achieving reactor outlet temperatures up to 1000 ^{o}C, in order to maximize hydrogen production efficiencies for either the SI or HTE-based processes. To reduce reactor vessel temperatures, the ATHENA model of the H2-MHR reactor system was modified to allow the reactor vessel inlet coolant to flow up through the central reflector rather than flowing up through the flow annulus between the core barrel and vessel wall, as in the current GT-MHR design. Figure 3 shows the ATHENA model of the H2-MHR core for the revised core inlet flow scheme.

Several ATHENA code calculations were performed for the revised flow configuration to evaluate the differences in system steady-state conditions and accident response with changes in flow configuration and coolant inlet temperature. The first set of calculations was performed assuming a center peaked axial power profile and a constant core exit temperature of 1000 ^{o}C. For this set of calculations, the central flow channel was simulated in ATHENA by removal of 7 graphite columns (out of a total of 61 columns) from the middle of the central graphite reflector. Calculations were performed for core inlet temperatures of 490 ^{o}C, 550 ^{o}C, and 600 ^{o}C, with core inlet flows adjusted to obtain the desired 1000 ^{o}C core outlet temperature. Results from these three cases were compared with those for a base case calculation assuming the standard MHR flow configuration and core inlet and outlet temperatures of 490 ^{o}C and 1000 ^{o}C, respectively.

The specific cases run in this first set of calculations were:

Case 1: Base case for H2-MHR with standard MHR inlet flow configuration and 490 ^{o}C core inlet temperature.

Case 2: Inlet flow routed through center reflector (7 reflector columns removed), with 490 ^{o}C core inlet temperature.

Case 3: Inlet flow routed through center reflector (7 reflector columns removed), with 550 ^{o}C core inlet temperature.

Case 4: Inlet flow routed through center reflector (7 reflector columns removed), with 600 ^{o}C core inlet temperature.

The results of these calculations, shown in Table 1, indicate that a significant reduction in the maximum average vessel wall temperature, when compared to the base case (Case 1), can be achieved by rerouting the coolant flow through the central reflector (last row of Table 1). However, this comes at the expense of an increase in pressure drop through the reactor core and vessel region, primarily because of the increase in pressure drop in the central reflector coolant channel. Increasing the core inlet temperature (and flow) to reduce the temperature rise through the core significantly increases the pressure loss through the MHR core and vessel region, but the increased helium flow rate reduces peak temperatures in the core because of the increased heat transfer to the coolant. Increasing the reactor inlet temperature also results in an increase in the maximum average steady-state reactor vessel wall temperature, but reactor vessel wall temperatures for each of the three cases with flow up the central-coolant channel remained well below the base case with the standard MHR inlet flow configuration.

Parameter	**Case 1**	**Case 2**	**Case 3**	**Case 4**
Core Power, MWt	600	600	600	600
Vessel Inlet Pressure, MPa	7.0	7.0	7.0	7.0
Vessel Inlet temperature, ^{o}C	490	490	550	600
Vessel Exit temperature, ^{o}C	1000	1000	1000	1000
Mass Flow rate, kg/s	228.6	229.3	259.8	292.2
Vessel differential pressure, kPa	38.2	52.7	69.5	89.7
Bypass flow, %	10.0	9.5	9.3	9.1
Peak fuel temperature, ^{o}C	1211	1208	1185	1167
Maximum average vessel wall temperature, ^{o}C	451	302	320	337

Table 1. Comparison of parameters for center flow configuration with variable coolant inlet temperatures and flow rates (center-peaked axial power profile).

In an attempt to reduce the pressure drop penalty associated with the coolant inlet flow through the central reflector, another calculation was performed using the coolant conditions corresponding to Case 4 in Table 1, but with nineteen fuel columns removed to provide a larger diameter flow channel through the central reflector. A comparison of this calculation with the results of Case 4 is shown in Table 2 below. With nineteen reflector columns removed, the pressure drop in the central flow channel was significantly reduced with only minor changes in peak fuel and reactor vessel wall temperatures.

Parameter	Seven central reflector columns removed (Case 4)	Nineteen central reflector columns removed
Core Power, MWt	600	600
Vessel Inlet Pressure, MPa	7.0	7.0
Vessel Inlet temperature, ^{o}C	600	600
Vessel Exit temperature, ^{o}C	1000	1000
Mass Flow rate, kg/s	292.2	292.6
Center flow channel ΔP, kPa (psid)	26.7 (3.9)	3.8 (0.6)
Active core ΔP, kPa (psid)	47.5 (6.9)	48.0 (7.0)
Vessel ΔP, kPa (psid)	89.7 (13.0)	67.2 (9.7)
Bypass flow, %	9.1	8.6
Peak fuel temperature, ^{o}C	1167	1165
Maximum average vessel wall temperature, ^{o}C	337	337

Table 2. Comparison of parameters for central flow channels with seven and nineteen reflector columns removed (center-peaked axial power profile).

Since the center-peaked axial power profile used in the above calculations is not expected to produce the highest peak fuel temperature, the two calculations presented in Table 2 were repeated with a bottom-peaked power profile. The results of these two calculations are shown in Table 3. As expected, the bottom-peaking power profile produced considerably higher peak fuel temperatures compared to the calculations with the center-peaked axial power profile, but did not significantly change other system parameters.

Parameter	Seven central reflector columns removed	Nineteen central reflector columns removed
Core Power, MWt	600	600
Vessel Inlet Pressure, MPa	7.0	7.0
Vessel Inlet temperature, ^{o}C	600	600
Vessel Exit temperature, ^{o}C	1000	1000
Mass Flow rate, kg/s	292.2	292.6
Center flow channel ΔP, kPa (psid)	26.7 (3.9)	3.79 (0.5)
Active core ΔP, kPa (psid)	46.6 (6.8)	47.0 (6.8)
Vessel ΔP, kPa	88.8 (12.9)	66.3 (9.6)
Bypass flow, %	9.1	8.6
Peak fuel temperature, ^{o}C	1229	1226
Maximum avg. vessel wall temperature, ^{o}C	336	336

Table 3. Comparison of parameters for central flow channels with seven and nineteen reflector columns removed (bottom-peaked axial power profile).

Finally, to determine the impact on a depressurized conduction cooldown transient with reactor scram, transient calculations were performed assuming a loss of coolant from steady-state conditions for a center-peaked axial power profile and central coolant channels corresponding to the removal of seven and nineteen graphite reflector columns, respectively (Table 2). The results of these calculations are shown in Figure 4. The figure shows that the reduced thermal mass in the core, associated with the removal of nineteen versus seven reflector

columns from the central reflector results in an increase in the peak fuel temperature from about 1775 K (1502 °C) for the case with 7 reflector columns removed, to 1820 K (1547 °C) for the case with 19 reflector columns removed.

Although the calculated average vessel temperatures during steady-state conditions and the calculated peak reactor core temperatures during depressurized conduction cool-down transients for the two cases above gave promising results, the excessive coolant pressure drop in the central flow channel during steady-state operation for the case with 7 reflector columns removed, and the potential effect on core neutronics for the case with 19 reflector columns removed made these coolant flow options less desirable. An additional calculation was therefore performed for the case with 7 reflector columns removed, but with a portion of the central column flow (25%) bypassed through the annulus between the core barrel and reactor vessel. While this flow scheme produced a lower coolant pressure drop through the central flow channel, even this relatively small amount of coolant inlet flow contacting the inner vessel wall appears to produce a significant increase in the average vessel wall temperature during steady-state operation.

To avoid the negative impacts associated with inlet coolant flow being routed up through the center reflector, an alternative cooling scheme was also evaluated in which the reactor coolant flow was routed upward between the outer core barrel and a cooling shroud installed between the core barrel and the inner reactor vessel wall to prevent the hot reactor cooling flow from directly contacting the vessel wall. To assist in cooling the inner vessel wall during normal operation, coolant from the compressor outlet, at a temperature of 140 °C, was routed up through a 0.015-m (0.59-in.) annular gap between the outer surface of the cooling shroud and the inner reactor vessel wall. This concept, however, would only be applicable to balance of plant designs involving electricity production with the standard MHR compressor and turbine-generator set, such as the HTE-based H2-MHR, or an SI-based H2-MHR that also produced electricity in a cogeneration mode. While this revised cooling scheme provides a mechanism for maintaining the reactor vessel at a lower temperature during normal operation, the installation of the cooling shroud introduces another barrier to heat transfer from the core to the reactor cavity cooling system during conduction cooldown events.

To evaluate vessel and core temperature responses during normal operation, and during high pressure conduction cooldown (HPCC) and low pressure conduction cooldown (LPCC) events, several different coolant flow rates were evaluated at different reactor core inlet and outlet temperatures to compare with results from the earlier studies. However, since the current reference core inlet and outlet temperatures have been established at 590 °C and 950 °C, respectively, only results for these reference design conditions are reported here. Table 4 summarizes the calculation results for normal operation with vessel cooling flows from the compressor outlet representing about 3%, 4% and 5% of the total core inlet flow for Cases 1, 2 and 3, respectively. A bottom-peaked axial power profile was used for each of these calculations.

	Case 1	Case 2	Case 3
Core inlet temp., °C	590	590	590
Core outlet temp., °C	950	950	950
Vessel cooling inlet temp., °C	140	140	140
Total core flow, kg/s	313.0	309.1	305.1
Vessel cooling flow, kg/s	9.6	12.8	16.0
Peak fuel temp., °C	1172	1174	1176
Max. avg. vessel wall temp., °C	378	356	338

Table 4. Calculated flows and temperatures for different reactor vessel cooling flows.

The last row of Table 4 shows that the maximum average vessel wall temperatures during steady-state operation for Cases 2 and 3 are below the ASME Code Case N-466-1 temperature of 371 °C. Since Case 2, requires the least amount of 140 °C cooling flow from the compressor outlet, additional transient calculations for both pressurized and depressurized conduction cooldown events with reactor scram were performed using initial steady-state conditions from this case. The low-pressure calculation assumed a rapid depressurization of the reactor system from steady-state operating conditions to atmosphere conditions in about 50 s, while the high-pressure calculations assumed a gradual depressurization to about 5 MPa over a period of about 70 hours (250,000 s). Peak fuel temperatures for these calculations are shown in Figure 5, and peak reactor vessel temperatures are shown in Figure 6. In these calculations, the peak fuel and reactor vessel temperatures both occur in the low-pressure transient. The peak fuel temperature of 1479 °C (1752 K) for the LPCC calculation occurred at approximately 60 hours (216,000 s) after the transient was initiated, and the peak fuel temperature of 1274 °C (1547 K) for the HPCC calculation occurred at approximately 67 hours (241,000 s) after transient initiation. In both cases, the calculated fuel temperature was below the peak design fuel temperature limit of 1600 °C.

The calculated peak reactor vessel temperatures shown in Figure 6 were 491 °C (764 K) for the LPCC calculation and 453 °C (726 K) for the HPCC calculation, and occurred at approximately 90 hrs (324,000 s) after transient initiation in both cases.

Although the above scoping calculations showed promising results in terms of reduced vessel and peak fuel temperatures during normal operation as well as during LPCC and HPCC transient events, the penalty on overall system performance associated with the 4% coolant bypass flow from the compressor outlet may preclude this option from consideration. Therefore, as the H2-MHR design evolves, this and other cooling options will continue to be evaluated to optimize plant design and performance during both normal operation and under accident conditions.

4. AVAILABILITY ASSESSMENT

Work has been initiated on the availability assessment of the SI-based H2-MHR plant concept using the INL developed SAPHIRE code [7]. The SAPHIRE (Systems Analysis Programs for Hands-on Integrated Reliability Evaluations) code refers to a set of several microcomputer programs that were developed to create and analyze probabilistic risk assessments (PRAs), primarily for nuclear power plants. The code evolved from the Integrated Reliability and Risk Analysis System (IRRAS) code, which is a state-of-the-art, microcomputer-based probabilistic risk assessment (PRA) model development and analysis tool. Like IRRAS, SAPHIRE is an integrated software tool that gives the user the ability to create and analyze fault trees and accident sequences using a microcomputer. It also provides functions that include graphical fault tree construction, cut set generation and quantification, and report generation. However, SAPHIRE also has a number of enhancements that provide a much more powerful and user-friendly system. In addition, the code runs under the Microsoft Windows operating system, taking advantage of the Windows graphical user interface (GUI).

The SAPHIRE model for the SI-based H2-MHR began with the development of a master fault tree for the SI process shown in Figure 2. The initial system configuration and component information for the master fault tree, shown in Figure 7, was obtained from General Atomics [8]. There are three transfer gates in the master fault tree that link to the individual fault trees for each of the chemical reaction sections in the SI process (i.e., the Bunsen reaction section, the H_2SO_4 decomposition section, and the HI decomposition section). The master fault tree, when linked to the individual fault trees for each of the three separate chemical reactions, provides the basis for evaluating and improving overall plant reliability, and assessing plant availability based on component failure rates and mission times. The fault trees for each of the three chemical reaction sections have been developed, but because of there complexity, are not shown here. A house event is also used with the transfer gate to provide the fault tree model with the capability to analyze each of the sections in the process flow sheets separately or together.

The complete SAPHIRE model that includes all three sections of the SI hydrogen production process has been developed in several steps. In the first step, models of each of the three sections of the SI process were developed using single components to perform each of the functions identified in the flow sheets in Reference 7. In the second step, these models were expanded to include multiple components to perform the different functions, based on the component parts lists contained in Tables 3-10 through 3-12 of the General Atomics report [8]. The third and final step was development of a refined model of one-fourth of the total system, by assuming four complete and identical hydrogen production systems were separately driven by the four modular helium reactors providing heat to the total hydrogen production process described in Reference 8.

The SAPHIRE model representing one-fourth of the complete hydrogen production plant currently consists of 27 fault trees, 115 sub-trees and 274 basic events. Three data bases were used to determine component failure rates. The Process Equipment Reliability Data by the Center for Chemical Process Safety (CCPS) [9] of the American Institute of Chemical Engineers includes accumulated and aggregated data from nuclear power plants, chemical process industries, offshore petroleum platforms, etc. The Offshore Reliability Data (OREDA) [10] covers reliability data from a wide range of equipment used in oil and natural gas exploration and production industries, as well as some onshore equipment. The European Industry Reliability Data Bank (EIReDA) [11] is the reliability database for the probabilistic safety assessment of nuclear power plants in France.

Using component failure rate data from the above data bases, hydrogen production plant failure rates have been developed using the SAPHIRE code. The failure data considered for this initial analysis include critical failures and degraded failures. Incipient failures, however, were not considered. The total number of cut sets (combinations of events leading to system failure) for the entire hydrogen production system is 1869. Out of this total number of cut sets, the top 27 cut sets account for ~96.3% of the total process system failure probability in a 24 hour operating period. As expected, initial results indicate that single failures of dynamic components (i.e., turbines, pumps, etc.) are the biggest contributors to the system failure probability.

The total failure probability of the hydrogen plant, based on the summation of all (1869) cut set failure probabilities, is calculated by SAPHIRE to be 0.0241 for a 24 hour mission time. This failure probability is considerably higher than that expected for the reactor power source. To reduce this failure probability, additional redundancies will need to be incorporated into the hydrogen production plant design, particularly for those components that are large contributors to the overall system failure probability. Therefore, as the conceptual design evolves, added redundancies as well as design improvements and enhancements will be evaluated using the SAPHIRE code, and where appropriate incorporated into the final plant conceptual design in order to achieve the desired hydrogen production plant reliability/availability.

5. HTE CONCEPT DEFINITION

A preliminary Mathcad model of a conceptual design for an HTE-based hydrogen production plant coupled to an

MHR was developed to perform initial sizing and sensitivity studies for the concept. Figure 8 shows the initial concept with calculated thermodynamic conditions identified on the flowsheet.

The preliminary flowsheet shown in Figure 1 includes an intermediate helium loop for transferring heat from the reactor power source to the water/steam supplying the electrolysis stack. This intermediate loop is included to preclude the potential for tritium migration from the reactor system to the product hydrogen gas. In addition, heat recovery from the hydrogen and oxygen product streams was used to improve overall hydrogen production efficiency. In this case, two heat exchangers were used to recover heat from the hydrogen stream and one heat exchanger was used to recover heat from the oxygen stream. For a 600 MWt reactor power source, this preliminary analysis indicates that approximately 43 MWt is required to heat the supply water/steam for the electrolysis stack to 850 ^{o}C. Assuming the electrolysis stack operates at a thermal-neutral voltage of 1.288 V at 850 ^{o}C (corresponding to an electrolysis thermal efficiency of 100%), the calculated rate of hydrogen production is 2.29 kg/s. For a lower heating value of, LHV_{H2} = -241,830 J/mol, the equivalent energy content of the hydrogen produced is approximately 277 MWt, corresponding to an overall hydrogen production plant efficiency of about 46%.

The results of this initial analysis are preliminary, since the calculations have not been thoroughly evaluated, and no attempt to optimize the system design was made. However, the results do provide a starting point for initial evaluation of system requirements and preliminary sizing of components. As the design evolves, refinements and improvements to the calculated system parameters will be made.

6. CONCLUSIONS

Results of analyses performed to date have shown that the high-temperature characteristics of the Modular Helium Reactor (MHR) make it an attractive candidate for the production of hydrogen using either thermochemical or high-temperature electrolysis processes. Preliminary flowsheet analyses performed for both the SI and HTE-based H2-MHR hydrogen production concepts indicate that large-scale hydrogen production efficiencies in the range of 50% can be realized.

The ATHENA code has been used to investigate alternative reactor primary system cooling schemes. Results of these thermal-hydraulic analyses demonstrate that alternative reactor cooling configurations can be effective in reducing peak fuel and vessel wall temperatures, but there are tradeoffs in overall plant performance and core neutronics that must be considered.

Initial SAPHIRE models of the three sections of the SI hydrogen production plant have been developed, and are being used in the plant design process to achieve desired plant reliability, availability, and maintainability goals. These SAPHIRE analyses are an integral part of the design process for both the SI and HTE-based H2-MHR design concepts and, as the designs evolve, will contribute to the overall optimization of these designs.

Although the HTE-based H2-MHR concept has not been developed to the extent that the SI-based concept has been developed, preliminary flowsheet analyses described in this paper indicate that the HTE-based H2-MHR design can achieve hydrogen production efficiencies comparable to those of the SI-based H2-MHR design.

REFERENCES

1. M. Richards and A. Shenoy, "Hydrogen Generation Using the Modular Helium Reactor," *Proceedings of the 12th International Conference on Nuclear Engineering*, April 25-19, 2004, Arlington, Virginia, American Society of Mechanical Engineers (2004).
2. M. Richards, A. Shenoy, and K. Schultz, "MHR-Based Hydrogen Production Systems," *Proceedings of the 2004 International Congress on Advances in Nuclear Power Plants(ICAPP '04),* June 13-17, Pittsburgh, PA, American Nuclear Society (2004).
3. M. Richards et. al., "Thermal Hydraulic Design of a Modular Helium Reactor Core Operating at 1000°C.
4. K. Carlson, P. A. Roth, and V. H. Ransom, "ATHENA Code Manual Volume I: Code Structure, System Models, and Solution Methods," EGG-RTH-7397, Idaho National Engineering Laboratory (1986).
5. The RELAP5-3D Development Team, "RELAP5-3D Code Manual, Volume 1: Code Structure, System Models and Solution Methods," INEEL-EXT-98-00834, Revision 1.1b, Idaho National Engineering and Environmental Laboratory (1999).
6. The RELAP5 Development Team, "RELAP5/MOD3 Code Manual, Volume 1: Code Structure, System Models, and Solution Methods," NUREG/CR-5535, INEL-95/0174, Idaho National Engineering Laboratory (1995).
7. K. D. Russell et al., "Systems Analysis Programs for Hands-on Integrated Reliability Evaluations (SAPHIRE) Version 5.0", NUREG-6116.
8. L. C. Brown et. al., "High Efficiency Generation of Hydrogen Fuels using Nuclear Power", GA-A24285, Rev.1, General Atomics (2002).
9. American Institute of Chemical Engineers (AIChE), "Guidelines for Process Equipment Reliability Data with Data Tables", Center for Chemical Process Safety (CCPS), (1989).
10. OREDA member companies, "Offshore Reliability Data", 4th Ed. (2002).
11. EIReDA, "European Industry Reliability Data Bank", 3rd Ed., Crete University Press (1998).

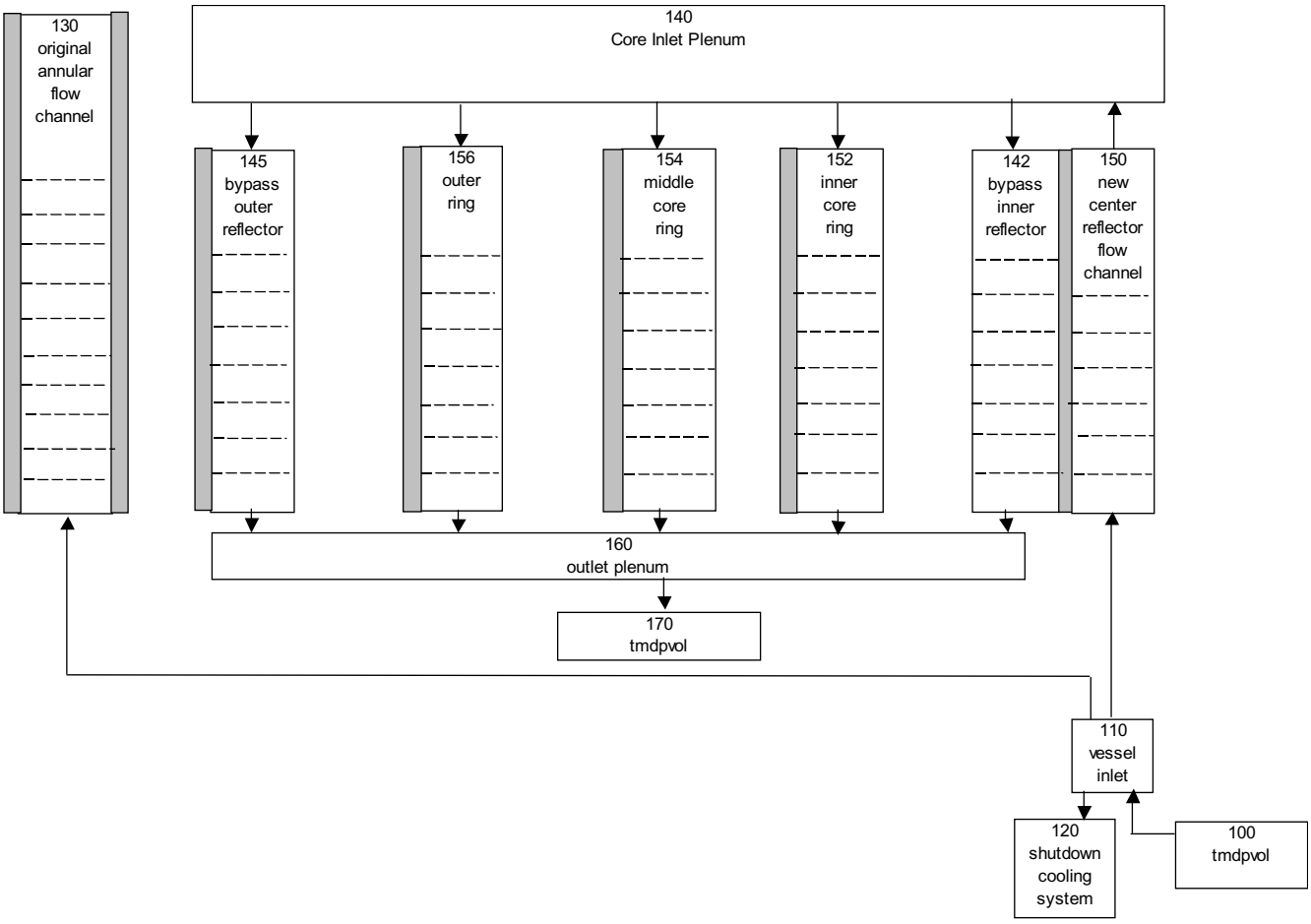

Figure 3. RELAP5/ATHENA model of H2-MHR with central flow channel.

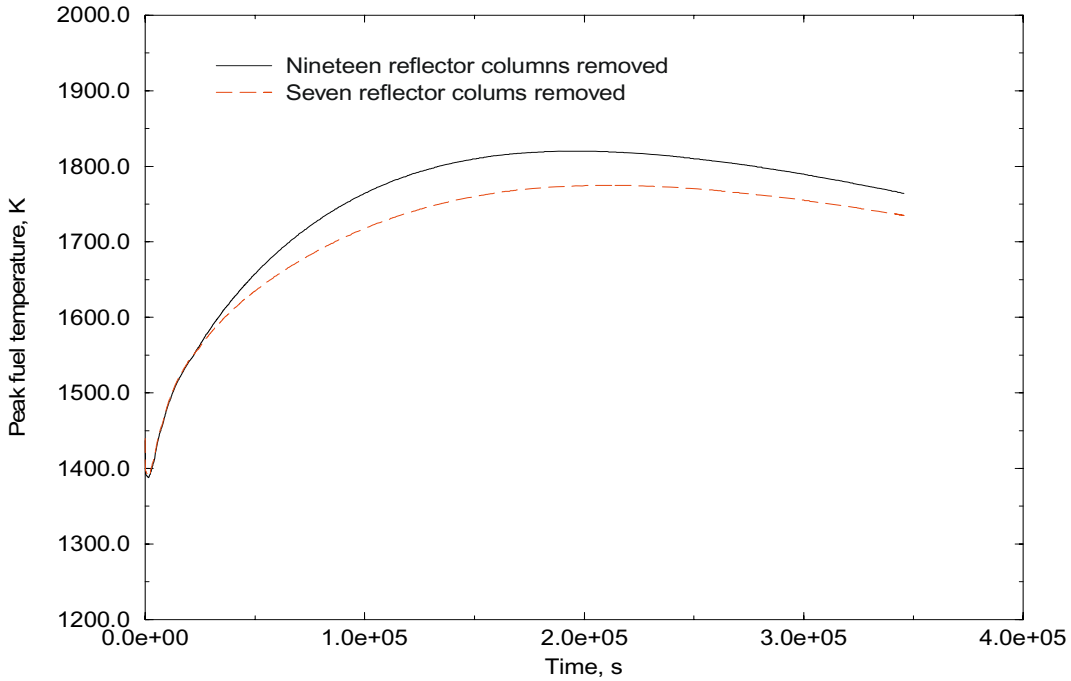

Figure 4. Peak conduction cool-down fuel temperatures with nineteen and seven graphite columns removed from central reflector region.

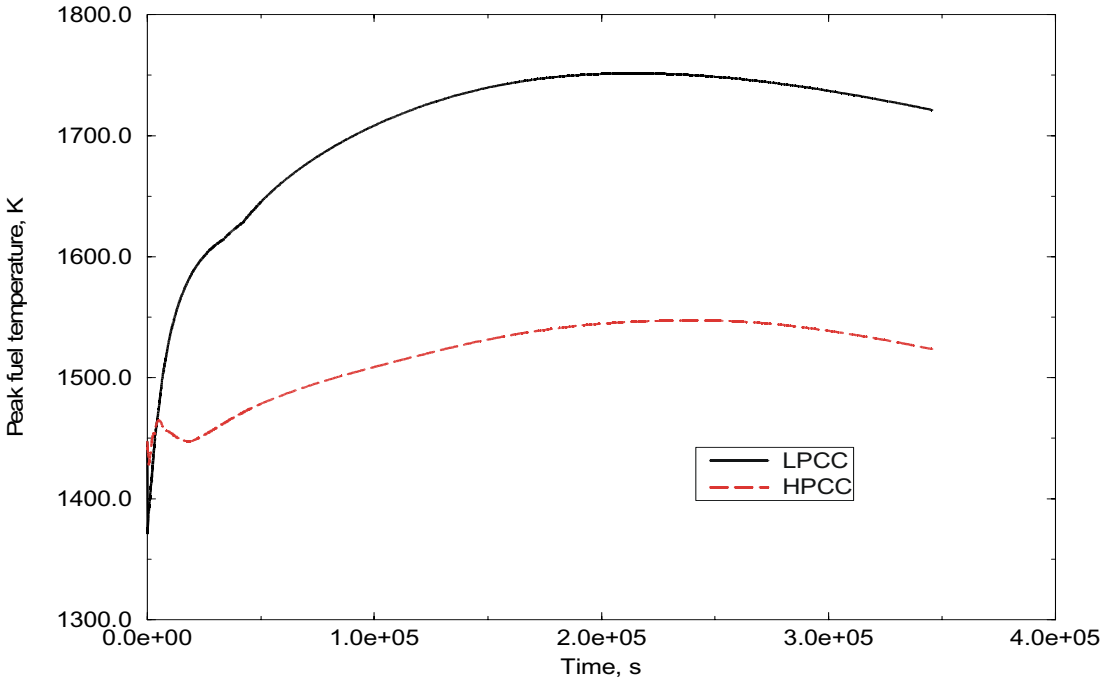

Figure 5. Calculated peak fuel temperature for pressurized and depressurized conduction cooldowns with reactor scram.

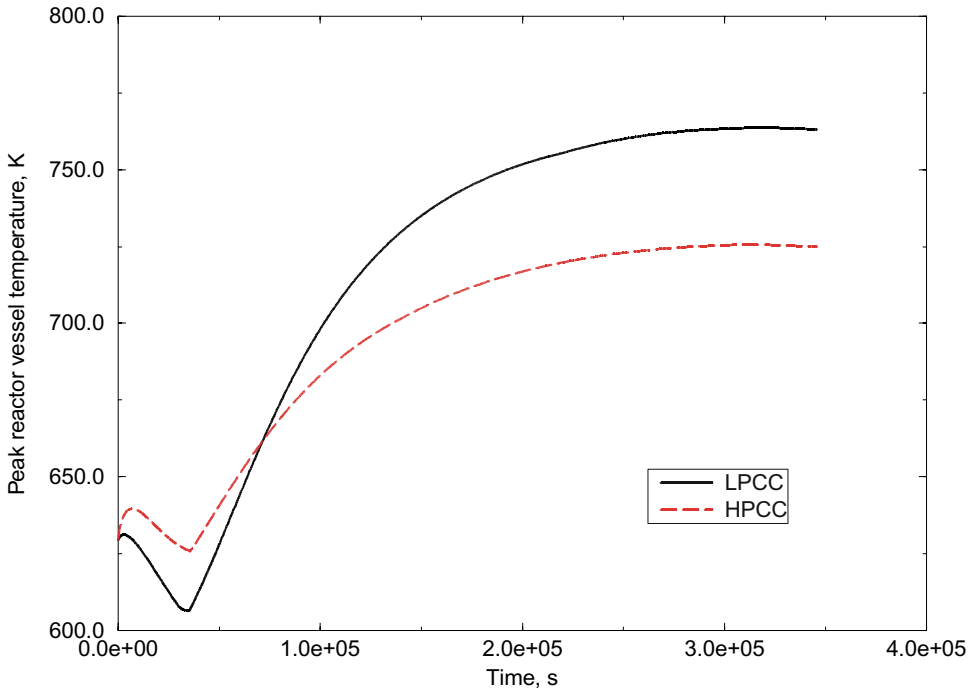

Figure 6. Calculated peak reactor vessel temperature for pressurized and depressurized conduction cooldowns with reactor scram.

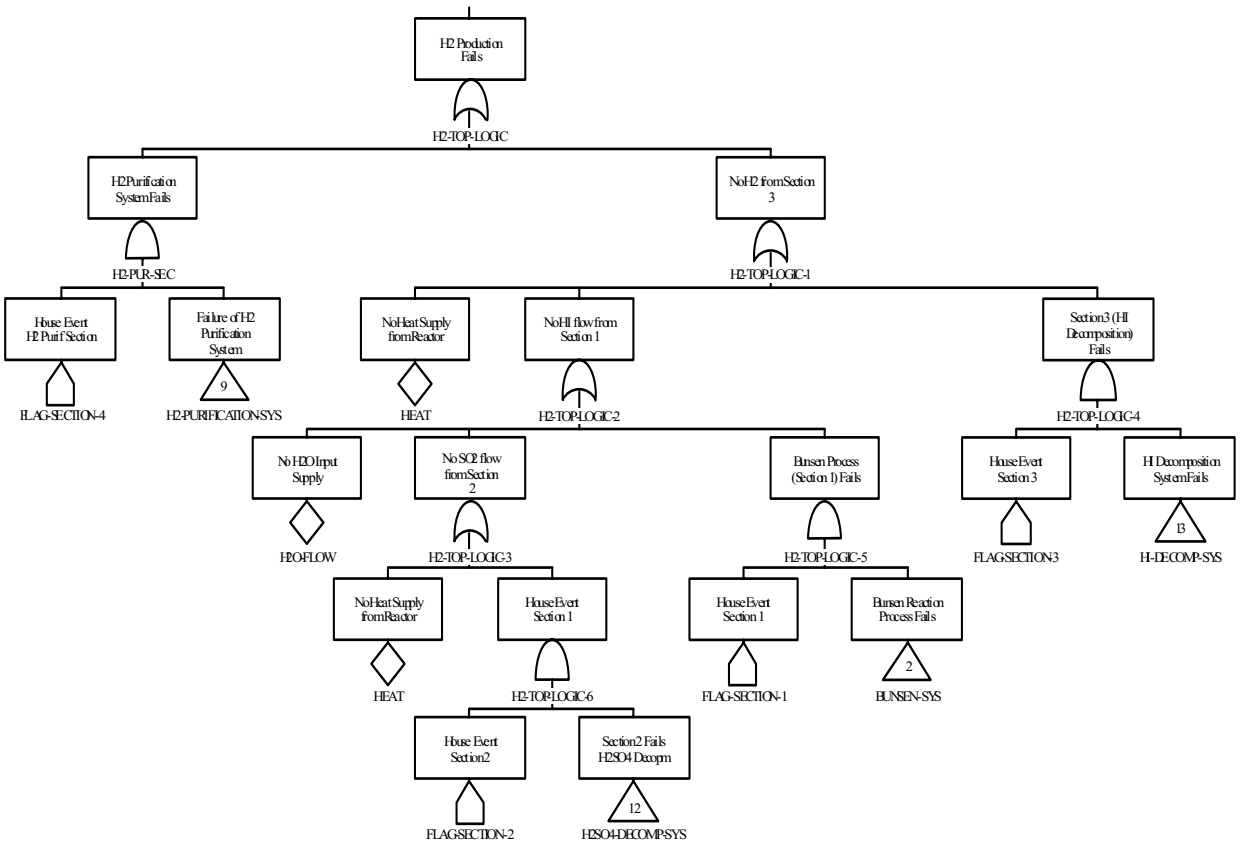

Figure 7. Master fault tree model for H_2 production plant.

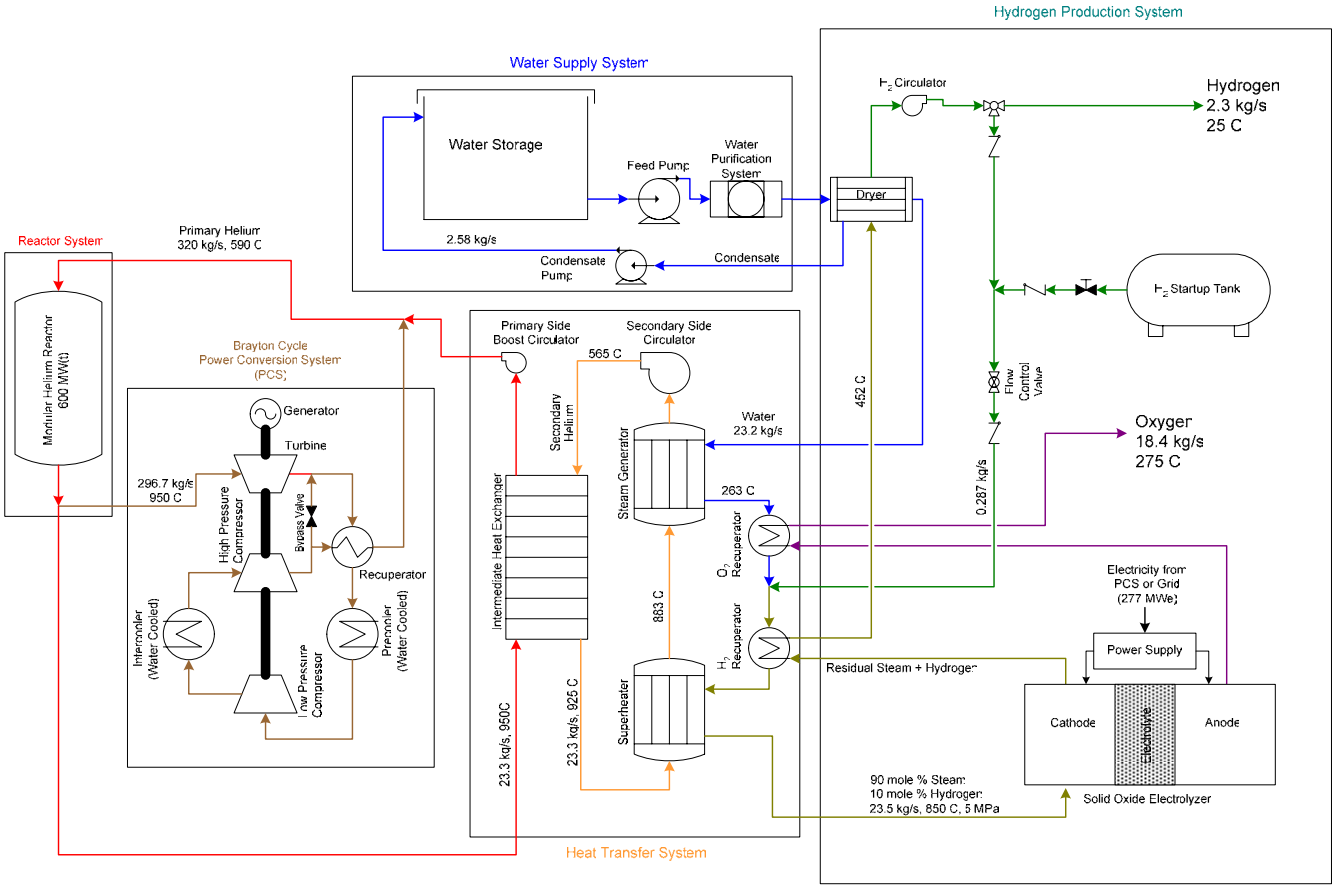

Figure 8. Flowsheet for high-temperature electrolysis plant coupled to the MHR.